JOURNAL OF MATERIALS SCIENCE 22 (1987) 2297–2304

TEM investigation of the tempering behaviour of the maraging PH 17.4 Mo stainless steel

C. SERVANT
Laboratoire de Métallurgie Structurale, Bât 413, UA CNRS 1107, Université Paris-Sud Centre d'Orsay, 91405 Orsay Cedex, France

EL H. GHERBI, G. CIZERON
Laboratoire de Structure des Matériaux Métalliques, Bât 465, Université Paris-Sud Centre d'Orsay, 91405 Orsay Cedex, France

The PH 17–4 Mo steel (Z6 CND 17.04.02), used in the steam generator of nuclear reactors, was investigated in order to determine the structural evolution occurring during tempering carried out under various conditions of duration and temperature. The formation and growth of different types of carbides such as Mo_2C, $M_{23}C_6$ and M_7C_3 and of Fe_2Mo intermetallic compound were studied and also of reversed austenite. A small secondary hardening peak was observed for tempering close to 400° C which is related to the Mo_2C carbide precipitation; beyond this temperature, softening occurs.

1. Introduction

During the last twenty years, due to the important requirements of the nuclear and aeronautical industries, the ferritic, austenitic, martensitic and austeno-martensitic stainless steels (with a tempering capacity) have undergone great development. It has been proved that among these different steels, the martensitic ones lead to the best compromise of the mechanical properties up to relatively high temperatures (1–5]. Furthermore, by annealing in the austenitic range these materials acquire a sufficient ductility to be machined; and besides, by tempering at moderate temperatures, nucleation and growth of very small precipitates occur in the martensite leading to an increase of the material hardness.

This paper describes various phenomena which occur during the tempering of a PH 17.4 Mo (Z 06 CND 17.04.02) stainless steel used in the steam generators of some nuclear reactors.

It may be mentioned that in an earlier work [6], carried out on the same steel, we especially described and analysed the structural evolutions occurring during different thermal treatments performed between 20 and 1400° C, using various heating and cooling rates.

2. Experimental procedure

2.1. Material

The chemical composition of the PH 17.4 Mo steel under consideration in the present paper is given in Tables I and II, respectively, for major and minor additions.

The steel, manufactured by Acieries Aubert et Duval (41 rue de Villiers, Neuilly-sur-Seine, BP120-92202, France), was provided as a bar of 80 mm diameter and 140 mm length. It was first solution-treated at 1020° C, then oil-quenched and aged at 580° C. In the following, this state will be referred to as the "as-received" state. As will be shown below, the duration of the industrial tempering carried out at 580° C has been deduced while comparing the microstructures of the as-received state with those of samples tempered at different temperatures (T_t) and for various times (t_t). Some samples in the as-received state were reheated at 1100° C for 30 min under argon atmosphere, then water-quenched. This state is further referred to the "as-quenched" state. It has been shown by optical microscopy that the steel in this state consists of lath martensite and δ-ferrite with a volume fraction of about 18%.

TABLE I Composition of PH 17.4 Mo steel for major additions

Elements	C	Cr	Ni	Mo
Composition (wt %)	0.051	15.95	4.65	1.24

2.2. Experimental methods

The structural evolutions of the steel studied in its different states were followed by

(i) differential dilatometric analysis, performed with a DPH 55 type dilatometer, under primary vacuum, with heating ($\dot{T}_h$) and cooling ($\dot{T}_c$) rates equal to 300 (° C) h^{-1}. The samples were 5 mm × 5 mm × 20 mm parallelepipeds;

(ii) thermomagnetic analysis carried out under primary vacuum in a Type II Adamel-Chevenard (ISA, Division Adamel et Lhomargy, Ivry-sur-Seine, France) apparatus, the heating and cooling rates being also both equal to 300 (° C) h^{-1}. The samples used were cylinders of 2 mm diameter and 10 mm length;

(iii) X-ray diffraction, performed with a Siemens apparatus using copper radiation filtered with a thin foil of pure iron; the set-up was equipped with a

0022–2461/87 $03.00 + .12

TABLE II Composition of PH 17.4 Mo steel for minor additions

Elements	Composition (wt %)	Elements	Composition (wt %)	Elements	Composition (wt %)
S	0.001	Nb	0.010	N	< 0.020
P	0.028	W	0.020	As	< 0.010
Si	0.370	V	0.035	Sn	< 0.005
Mn	0.785	Cu	0.070	Sb	< 0.002
				Pb	< 0.003

crystal of graphite used as a back monochromator;

(iv) hardness measurements under a 300 N force carried out on a Malicet and Blin (Société Malicot et Blin SKF, Ivry-sur-Seine, France) apparatus;

(v) electron microscopy and microdiffraction, in a Jeol 100C at 100 kV. Thin foils were obtained using a Struers device (dual jet electropolishing technique) at 60 V with a current density of 0.2 A cm^{-2}, in a bath kept at $-8°$ C, and containing 725 cm^3 methyl alcohol, 175 cm^3 ethylene glycol monobutylic ether and 100 cm^3 perchloric acid.

3. Experimental results

3.1. Dilatometric and thermomagnetic analysis

The differential dilatometric curve recorded with $\dot{T}_h = 300\,(°\,C)\,h^{-1}$ (Fig. 1) shows the dimensional variations developed in the as-quenched sample. Indeed, it can be noticed that the curve exhibits a slight curvature between 100 and 250° C corresponding to a transient increase of the mean expansion coefficient of the sample. This can be related to the diminution of the residual stresses formed during the prior martensitic transformation. Then from the A_{c_d} point (which is equal to 620° C for $\dot{T}_h = 300\,(°\,C)\,h^{-1}$) a strong contraction reveals the austenitic transformation until the A_{c_f} point (equal to 965° C for this particular $\dot{T}_h$). During the cooling, we only observe the martensitic transformation starting at the M_S point, at 150° C; this transformation appears by a strong expansion. The M_f point is slightly higher than 20° C. The use of the A_{c_d}, A_{c_f}, M_S and M_f points instead of the A_{c_1}, A_{c_3}, A_{r_1}, and A_{r_3} temperature can be justified by the fact that pearlite transformation does not occur in the case of PH 17.4 Mo steel.

The thermomagnetic curve recorded by using the same heating rate is shown in Fig. 2. It only exhibits before the A_{c_d} point an increase of the magnetic intensity mainly beyond 350° C; this behaviour corresponds to a change in the size of the Weiss domains [6, 7] rather than to a change in composition of the martensitic matrix. Therefore the comparison of the thermomagnetometric curve shown in Fig. 2 and those recorded on steels having a different composition of PH 17.4 Mo steel [8] shows that PH 17.4 Mo steel does not contain enough carbon to lead to the formation of ε or Fe_3C carbides in the martensite. Indeed, no noticeable contraction corresponding to such precipitates was observed for temperatures lower than 300° C on the dilatometric curve shown in Fig. 1. The decrease of the magnetic intensity observed in two successive stages beyond the A_{c_d} point has been related to various phenomena and has been widely analysed in a previous paper [6]. We can briefly summarize it as follows.

Before the A_{c_d} point, precipitation phenomena occurring in the martensitic matrix (discussed in the next section) lead to a heterogeneity in this phase as far as the addition element content is concerned: i.e. M_i zones are respectively enriched (M_{E_i}) or depleted (M_{D_i}) in these elements, particularly (Ni + Mo). Beyond the A_{c_d} point, these two sets of martensites transform into austenite in two successive stages according to a decomposition mechanism which is similar to the one occurring in the case of a metastable phase diagram for which diffusion processes take place, according to the relations

$$\text{1st stage: } M_{E_i} \rightarrow \gamma_{EE_i} + M_{ED_i} \qquad \gamma_{ED_i}$$

$$\text{2nd stage } M_{D_i} \rightarrow \gamma_{DE_i} + M_{DD_i} \qquad \gamma_{DD_i}$$

The first decrease of the magnetic intensity observed in Fig. 2 from the A_{c_d} point is reversible and has been

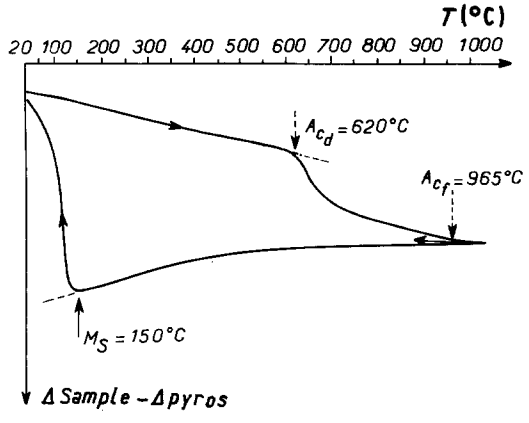

Figure 1 Differential dilatometric curve recorded from a sample in the as-quenched state with heating and cooling rates of 300 (° C) h^{-1}. Δ Sample = $[(L_T - L_0)/L_0]$ where L_T is length at temperature T, and L_0 is length at 20° C.

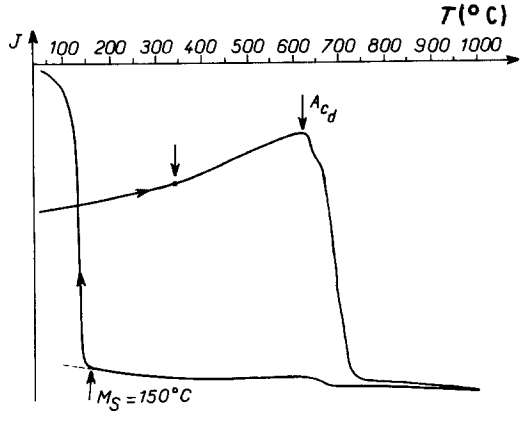

Figure 2 Thermomagnetic curve recorded from a sample in the as-quenched state with heating and cooling rates of 300 (° C) h^{-1}.

interpreted as the Curie point of the γ_{EE_i} phases and of the δ-ferrite; the second decrease of the magnetic intensity, which is also reversible, corresponds to the Curie points of the martensites of different compositions such as M_{ED_i}, and M_{E_i}.

3.2. TEM results

Examinations of the PH 17.4 Mo steels under TEM and for the three states (as-quenched, as-tempered and as-received) have been made at 20° C.

3.2.1. As-quenched state

The microstructure consists only of two phases: a lath martensitic matrix containing a high density of internal dislocations. The laths either show between them a very slight desorientation and form packets, or they are twin-related. They exhibit a variable size: indeed the largest dimension can vary from 40 to 0.5 μm. Very rarely, thin microtwins are identified inside the laths of martensite, and a δ-ferrite with a dislocation density which is less than that observed in the lath martensite.

3.2.2. As-tempered state

Various isochronal and isothermal tempering treatments have been carried out on samples in the as-quenched state. Precipitates of different natures such as carbides, σ phase and Laves phase have been revealed either in the martensitic matrix or in the δ-ferrite as a function of the tempering parameters (T_t and t_t). Furthermore, a partial transformation of the martensite into austenite as well as precipitation into the γ phase was also observed.

3.2.3. Precipitation of carbides

The *isochronal treatments* were performed for 70 h at temperatures lower (520–550–575–600° C) or higher (650–700–750–800–850–900–950° C) than the A_{c_d} point (620° C). First, no carbide precipitation of the $M_{23}C_6$ type was observed after the different tempering treatments carried out at $T_t < 550$° C. When T_t reaches 570° C, a few $M_{23}C_6$ carbides with a very small size ($\bar{S} \simeq 20$ nm) are visible as can be seen in Figs 3a and b. In order to increase the volume fraction and in particular the size of these carbides, it is necessary to temper the material at a temperature significantly higher than the A_{c_d} point, ranging from 700 to 850° C (see for example Figs 4a and b: the mean size, $\bar{S}$, of the $M_{23}C_6$ carbides then reaches about 200 nm). They are localized generally at the boundaries of the laths of martensite which is not yet transformed into austenite.

The *isothermal treatments* were carried out at 570° C. This particular temperature was chosen because it corresponds to the industrial tempering range (as-received state):

(i) after a tempering time of 5 h, only rare and very small $M_{23}C_6$ carbides are formed inside the laths of martensite and/or at their boundaries;

(ii) when t_t is equal to 25 h, the $M_{23}C_6$ carbides present a larger size and are mainly located at the lath boundaries (Fig. 5a);

(iii) for $t_t > 25$ h, the precipitation of $M_{23}C_6$ becomes more important; these carbides are located at the lath martensite boundaries (and/or at the martensite–austenite interfaces) (Fig. 5b). Indeed, for such isothermal ageing conditions, reversed austenite is already formed at a temperature lower than that of the A_{c_d} point (620° C) determined in dynamic conditions for $\dot{T}_h = 300$ (° C) h^{-1}.

(iv) When t increases and reaches 1000 h, $M_{23}C_6$ carbide also precipitates inside the δ-ferrite (Fig. 5d).

3.2.4. Precipitation of the Laves phase

The precipitation was followed during the isothermal tempering treatment carried out at 570° C on the as-quenched sample, and has been observed for relatively long tempering durations ($\simeq 1000$ h). The Fe_2Mo precipitates, which are rare, either

(i) have a globular shape and are situated in the martensitic matrix (see A in Fig. 6a) and/or inside the

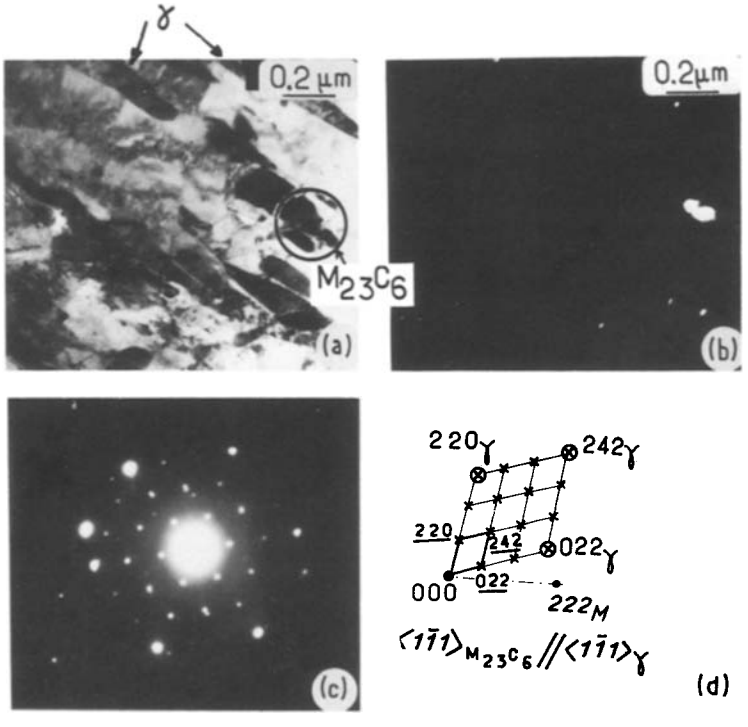

Figure 3 Microstructure of the as-quenched sample, tempered 70 h at 570° C. (a) Bright field showing the $M_{23}C_6$ carbides; (b) dark field on the same area obtained from a reflection spot of the $M_{23}C_6$ carbide; (c) diffraction pattern obtained on the circled area, with a $\langle 1\bar{1}1\rangle_{M_{23}C_6}$ zone axis; (d) key to (c) (○) γ, (×) $M_{23}C_6$ (reflections underlined).

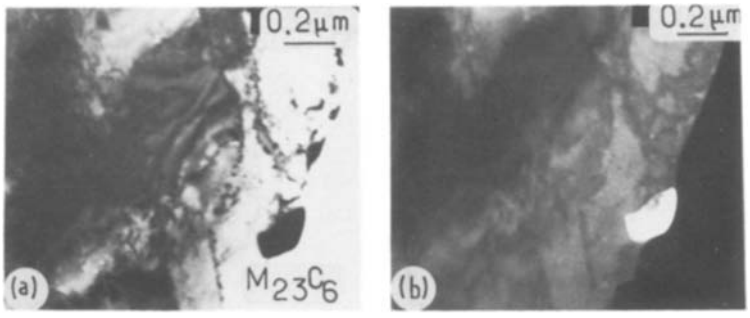

Figure 4 Microstructure of the as-quenched sample, tempered 70 h at 700° C. (a) Bright field showing the growth of $M_{23}C_6$ carbides; (b) dark field on the same area obtained from a reflection spot of the $M_{23}C_6$ carbide.

δ-ferrite; or

(ii) are elongated in shape (see B in Figs 6a and b) and are situated at the interfaces of the laths of martensite or at the martensite/δ-ferrite interface.

It can be noted that the diffraction patterns obtained from the Fe_2Mo precipitates exhibit streaking through certain diffraction spots (Fig. 6c), which is due to the polytypism presented by these intermetallic compounds as described by Allen *et al.* [9]. In fact in the dark field shown in Fig. 6b there can be noticed the existence of small faulted domains, the larger dimensions of which are perpendicular to the streaks seen in the diffraction pattern shown in Fig. 6c.

3.2.5. Formation of σ phase

For isochronal treatments of 70 h, we have shown that it was necessary to use a relatively high temperature (850° C) in order to promote the formation of the σ phase. As shown in Fig. 7, the σ phase particles, which are mainly located between packets of laths, reach an important size for this duration of thermal treatment, and their shape is rather irregular. When the temperature is increased up to 950° C, the σ phase dissolves.

3.2.6. Formation of reversed austenite

The respective evolutions of the X-ray diffraction peaks of the reversed austenite and martensite for isothermal treatments carried out at 520 and 570° C are shown in Fig. 8. It will be noted that the {1 1 1} reflection of austenite only appears when T_t reaches 570° C and t_t is longer than 10 h.

The change in the morphology and the amount of the reversed austenite retained at room temperature are shown in Fig. 9 for T_t = 570° C. After 70 h, the γ phase appears to be largely situated at the boundaries of the laths of martensite (Fig. 9a); for t_t = 280 h, the volume fraction of the γ phase is $\simeq 4\%$ and furthermore its distribution in the thin foils of the tempered sample is heterogeneous, as it can be seen in Fig. 9b. In fact, in this figure it can be noted that the volume fraction of the γ phase is greater than the average volume fraction of the γ phase. The reversed austenite formed during the tempering treatment and retained until 20° C or below is related to its additional elements (Ni + Mo) content [6]. After tempering of 1000 h, a significant grain growth takes place in the γ phase as shown in Fig. 9c.

3.3. Hardness measurements

Changes in hardness were followed in the as-quenched samples aged for two hours at different temperatures ranging from 20 to 600° C. As revealed in Fig. 10, up to 300° C the hardness is very slightly decreasing: this fact can be related to the softening of the martensitic matrix due to both the elimination of internal stress and the decrease in the dislocation density. On the other hand, when the tempering is carried out at higher temperatures the hardness is slightly increasing ($\simeq$ 30 DPH units) and then exhibits a maximum when

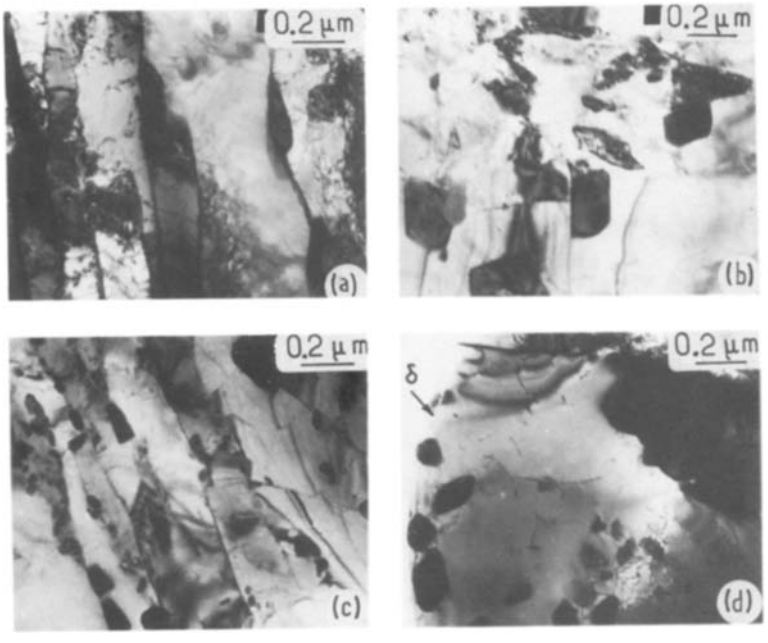

Figure 5 Microstructure of the as-quenched sample, tempered at 570° C during duration t equal to (a) 25, (b) 280 and (c, d) 1000 h. Bright fields showing the $M_{23}C_6$ carbides located at lath boundaries (a, b, c) and in the δ-ferrite (d).

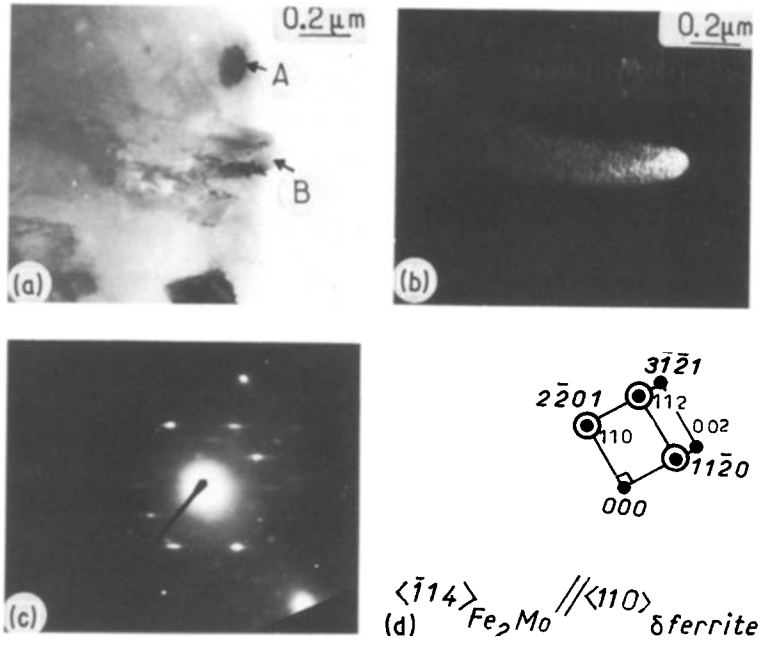

Figure 6 (a, b) Bright and dark fields showing the Fe_2Mo precipitates; (c) diffraction pattern with a zone axis $\langle \bar{1}\,1\,4\rangle_{Fe_2Mo} \| \langle 1\,1\,0\rangle_{ferrite}$; (d) key to (c): (●) δ-ferrite, (⊙) Fe_2Mo.

$T \simeq 400°C$. This secondary hardening peak with a small amplitude can be related to the precipitation of very tiny Mo_2C carbides. It has been shown by Honeycombe and Seal [10] and Smith and Nutting [11] that an incubation time is observed, preceding the formation of this type of carbide and longer as T_t was higher.

For tempering temperatures higher than 400 to 450° C, the alloy softens; this over-ageing is able to provoke a decrease of about 100 in the DPH value.

3.3.1. As-received state

In this state, three phases are simultaneously shown by TEM experiments: lath martensite, δ-ferrite (with a volume fraction of $\simeq 21\%$ determined from optical micrographs) and reversed austenite (with a volume fraction $\leqslant 3\%$). In fact, by X-ray diffraction analysis it is not possible to distinguish the diffraction peaks of the two bcc phases (martensite and δ-ferrite) due to the very small difference between their respective cristalline parameters. Furthermore, the presence of mainly globular and of variable-size $M_{23}C_6$ were observed (Figs 11a and b); they are mainly located at the lath martensite boundaries. It is at the martensite–δ-ferrite interfaces that the biggest $M_{23}C_6$ precipitates have been seen. Moreover, $M_{23}C_6$ carbide precipitates have been detected inside the reversed austenite or at the austenite–martensite interfaces, as shown in Figs 12a and b. We have found the orientation relationship discussed by Lewis and Hattersley [12] between the reversed austenite and the $M_{23}C_6$ precipitate:

$$\{1\,0\,0\}_\gamma \| \{1\,0\,0\}_{M_{23}C_6} \quad \text{and} \quad \langle 0\,0\,1\rangle_\gamma \| \langle 0\,0\,1\rangle_{M_{23}C_6}$$

The reversed austenite is formed from the martensite with the classical orientation relationship of Kurdjumov and Sachs [13].

σ

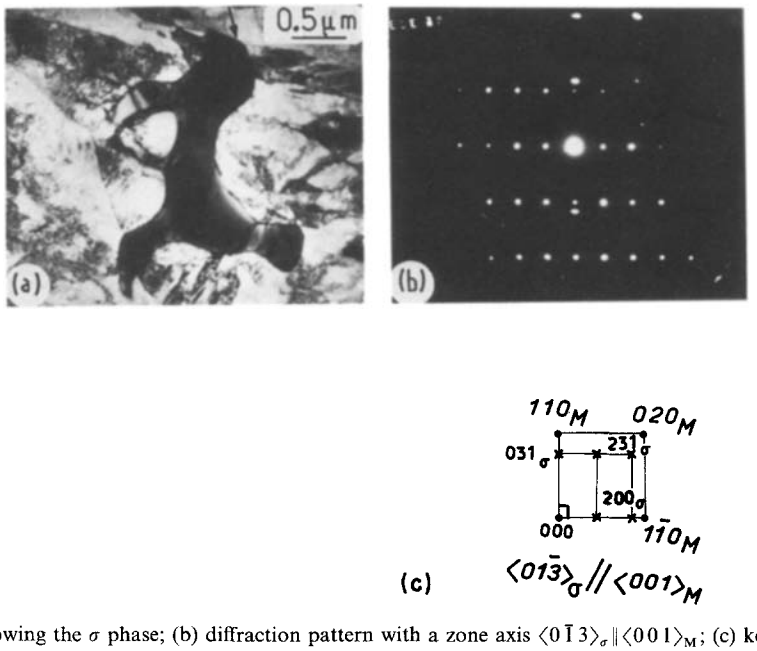

Figure 7 (a) Bright field showing the σ phase; (b) diffraction pattern with a zone axis $\langle 0\,\bar{1}\,3\rangle_\sigma \| \langle 0\,0\,1\rangle_M$; (c) key to (b).

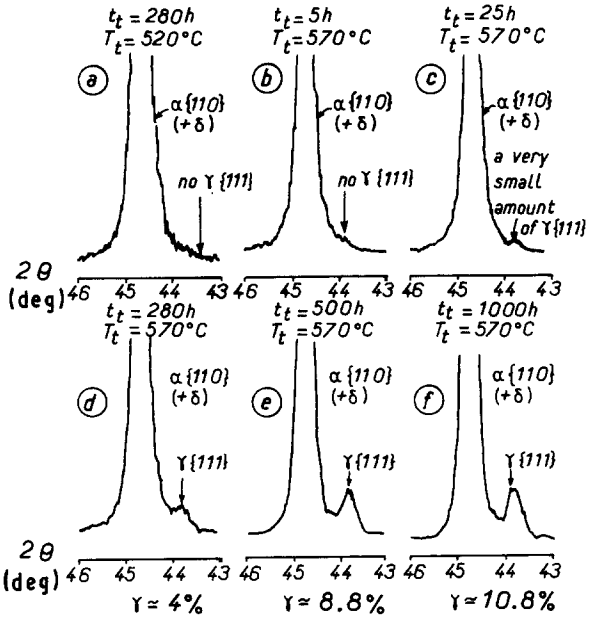

Figure 8 X-ray diffraction patterns showing the evolution of the reversed austenite.

$$\{1\,1\,1\}_\gamma \| \{1\,1\,0\}_M \quad \text{and} \quad \langle 1\,\bar{1}\,0\rangle_\gamma \| \langle 1\,\bar{1}\,1\rangle_{M_{23}C_6}$$

It has been concluded that the duration of the industrial tempering was approximately equal to ten hours, due to the presence of a small amount both of the γ phase and $M_{23}C_6$ carbides in the as-received state. We may also mention that some globular M_7C_3 carbides were observed inside the laths of martensite, or at the martensite–δ-ferrite interfaces (Figs 11c, d and e). Their size is noticeably bigger than that of the $M_{23}C_6$ carbides. They have probably been formed during the solidification process of the alloy since in the as-quenched samples tempered later on; their formation was detected only after $t_t \geqslant 70$ h at $T_t = 570°$ C.

4. Conclusions

Tempering carried out on PH 17.4 Mo steel causes

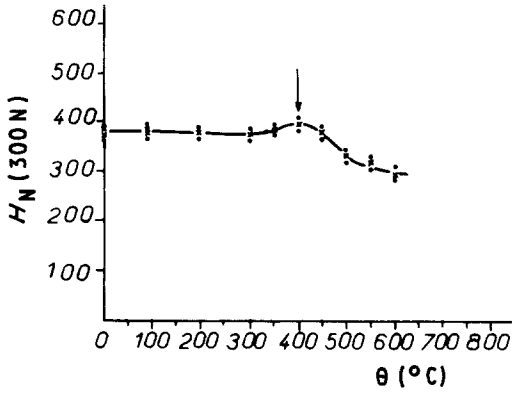

Figure 10 Hardness changes for isochronal ageing duration of 2 h as a function of increasing temperature; samples initially in the as-quenched state.

structural evolution in the martensite as well as in the δ-ferrite (the volume fraction of δ phase is $\simeq 18\%$ in the as-quenched state and $\simeq 21\%$ in the as-received state). However, in these two phases the precipitation is very different in type, in the T_t temperature range and in the tempering time (t_t) required. According to the values of these parameters, T_t and t_t, we have observed the formation and growth of different types of phase, such as the following:

1. Carbides of various natures:

(i) Mo_2C, in the temperature range 350 to 500° C. The presence of these very small carbides only gives a secondary hardening peak, with a small amplitude; the corresponding increase is in fact limited to about 30 DPH units.

(ii) $M_{23}C_6$ in the temperature range 550 to 900° C, both in the martensite and in the δ-ferrite.

(iii) M_7C_3 for $T_t > 570°$ C and $t > 70$ h.

2. Intermetallic compound Fe_2Mo, in the temperature range 500 to 650° C and for long tempering durations. The formation of σ phase was also detected for temperatures much higher than the A_{c_d} point

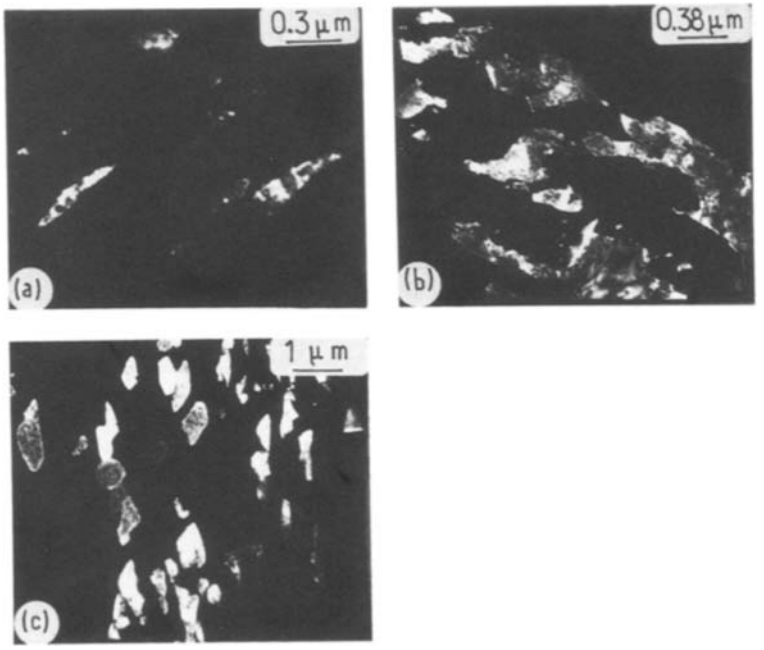

Figure 9 Dark-field electron micrographs showing the evolution of reversed austenite at 570° C for increasing tempering duration: (a) 70 h, (b) 280 h, (c) 1000 h.

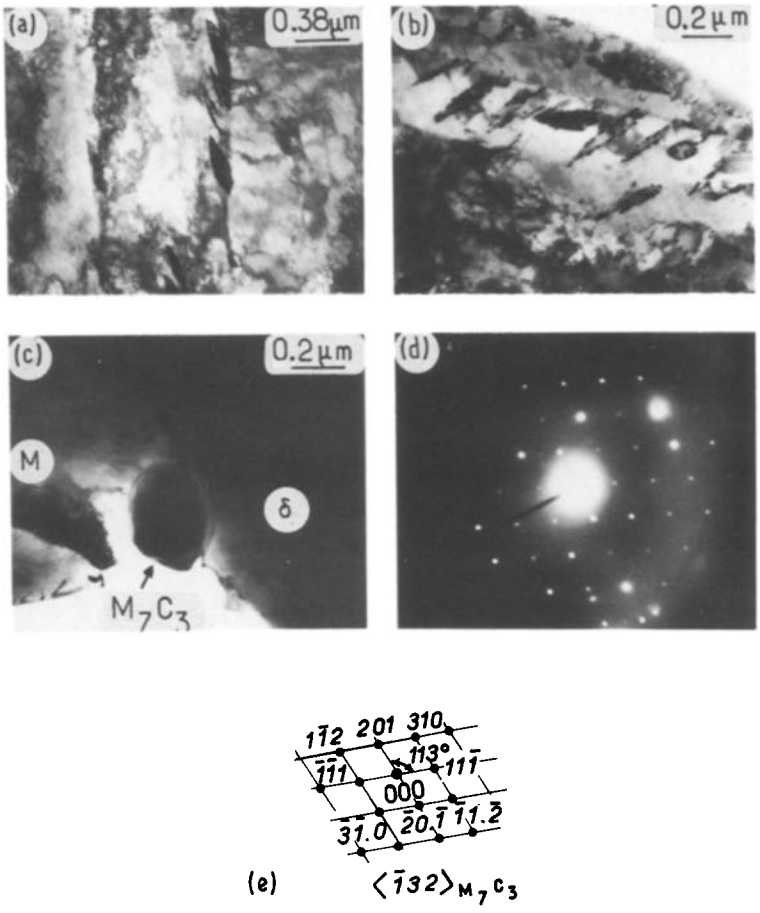

Figure 11 Microstructure of the as-received state. (a, b) Bright fields showing the $M_{23}C_6$ carbides at the boundaries of the laths; (c) bright fields showing a coarse M_7C_3 carbide situated at the martensite–δ-ferrite interface; (d) diffraction pattern with a $\langle \bar{1}\,3\,2\rangle_{M_7C_3}$ zone axis; (e) key to (d).

temperatures equal or superior to 850° C); this phase is no longer stable when the temperature becomes higher than 950° C and turns into the austenitic solid solution.

3. Reversed austenite for $T_t \geqslant 570°$ C.

It can therefore be concluded that during the industrial use of PH 17.4 Mo steel in steam generators below 550° C, the precipitation of $M_{23}C_6$ carbides and of Fe_2Mo intermetallic compound occurs either in the laths of martensite, in the δ-ferrite or at their interface. However the volume fraction of carbides which precipitates is low although higher than the volume of other precipitates.

In the future, it will be of interest to characterize the influence of the structural evolutions described in the above sections on the mechanical properties of the steel, especially on the creep behaviour. In particular, it will be important to determine the influence of the

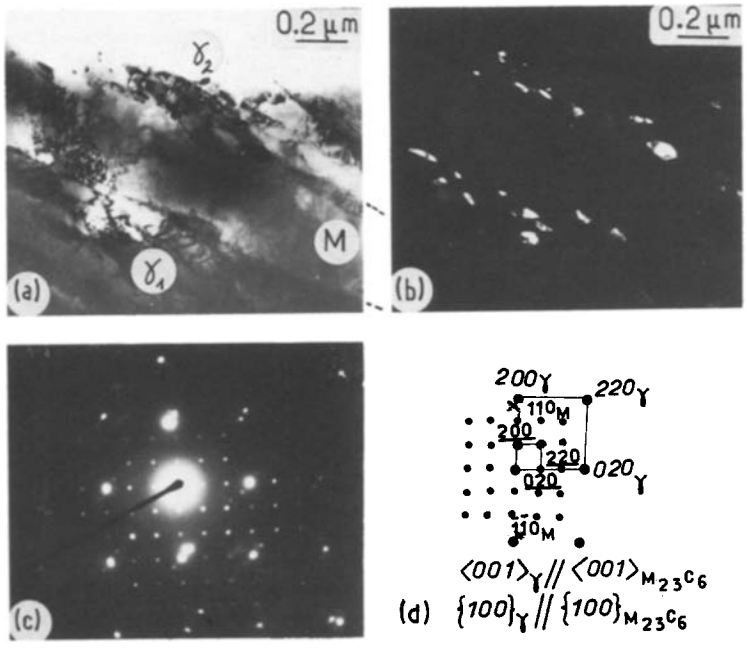

Figure 12 (a) Bright field showing the $M_{23}C_6$ carbides inside the austenite and at the austenite–martensite interface; (b) dark field on the same area (c) diffraction pattern with a zone axis $\langle 0\,0\,1\rangle_\gamma \parallel \langle 0\,0\,1\rangle_{M_{23}C_6}$; (d) key to (c): (●) γ, (x) M, $M_{23}C_6$ reflections underlined.

slow depletion of molybdenum from the matrix which occurs for long tempering durations.

References

1. P. PATRIARCA, *Nucl. Tech.* **28** (1976) 516.
2. M. CAUBON and L. MATHONET, *Rev. Met.* **5** (1969) 345.
3. Ph. BERGE, J. GARAUD and P. PONCIN, in Proceedings of BNES International Conference on Ferritic Steels for Reactors in Steam Generators, London, May 1977.
4. K. J. IRVINE, F. B. PICKERING and D. J. CROWE, *J. Iron Steel Inst.* **8** (1960) 386.
5. R. TRICOT and R. CASTRO, *Mem. Sci. Rev. Met.* **7/8** (1966) 657.
6. C. SERVANT, EL H. GHERBI and G. CIZERON, *Matér. Techn.* September/October (1986) 405.
7. A. HERPIN, "Théorie du magnétisme" (Presses Universitaires de France, Paris 1986).
8. E. R. PETTY, "Martensite fundamentals and technology" (Longman, London, 1970).
9. C. W. ALLEN, P. DELAVIGNETTE and S. AMELINCKX, *Phys. Status Solidi (a)* **9** (1972) 237.
10. R. W. HONEYCOMBE and A. D. SEAL, *J. Iron Steel Inst.* **188** (1958) 9.
11. E. SMITH and J. NUTTING, *ibid.* **187** (1957) 314.
12. M. H. LEWISS and B. HATTERSLEY, *Acta Metall.* **13** (1965) 1159.
13. G. KURDJUMOV and G. SACHS, *Z. Physik* **64** (1930) 325.

Received 26 March
and accepted 11 November 1986